

Mo₆Ga₃₁ endohedral cluster superconductor

Valeriy Yu. Verchenko,^{1,2} Alexander O. Zubtsovskii,^{1,3} Alexander A. Tsirlin,³
Zheng Wei,⁴ Maria Roslova,⁵ Evgeny V. Dikarev,⁴ and Andrei V. Shevelkov¹

¹*Department of Chemistry, Lomonosov Moscow State University, 119991 Moscow, Russia*

²*National Institute of Chemical Physics and Biophysics, 12618 Tallinn, Estonia**

³*Experimental Physics VI, Center for Electronic Correlations and Magnetism,
Institute of Physics, University of Augsburg, 86135 Augsburg, Germany*

⁴*Department of Chemistry, University at Albany, SUNY, Albany, 12222 New York, United States*

⁵*Department of Materials and Environmental Chemistry,
Stockholm University, SE-106 91 Stockholm, Sweden*

Synthesis, crystal and electronic structure, and physical properties of the Mo₆Ga₃₁ endohedral cluster superconductor are reported. The compound has two crystallographic modifications, monoclinic and triclinic, in which the same {Mo₁₂Ga₆₂} building units are perpendicular or codirectional to each other, respectively. Monoclinic and triclinic structures of Mo₆Ga₃₁ possess qualitatively the same electronic density of states showing a high peak at the Fermi level. Both modifications are inherently present in the bulk specimen. Due to the proximity effect, bulk Mo₆Ga₃₁ exhibits single superconducting transition at the critical temperature of 8.2 K in zero magnetic field. The upper critical field, which is 7.8 T at zero temperature, shows clear enhancement with respect to the Werthamer-Helfand-Hohenberg prediction. Accordingly, heat capacity measurements indicate strong electron-phonon coupling in the superconducting state with the large ratio of $2\Delta(0)/(k_B T_c) = 4.5$, where $2\Delta(0)$ is the full superconducting gap at zero temperature.

I. INTRODUCTION

Recently, the transition metal-embedded Ga clusters were proposed as a structural motif favorable for superconductivity.¹ Endohedral Ga clusters centered by atoms of $4d$ or $5d$ transition metals can be found in the crystal structures of Ga-rich binary intermetallic compounds, among which Mo₈Ga₄₁ with $T_c = 9.8$ K,² Mo₆Ga₃₁ (8 K),³ Mo₄Ga_{21-x-δ}Sn_x (5.85 K),⁴ ReGa₅ (2.3 K),¹ Rh₂Ga₉ (1.9 K),⁵ and Ir₂Ga₉ (2.2 K)⁵ exhibit superconducting properties. In this list, the Mo-based superconductors are distinguished by higher critical temperatures. A closer look reveals that they possess non-trivial superconducting-state properties deviating from the Bardeen-Cooper-Schriber (BCS) model.

For Mo₈Ga₄₁, measurements of heat capacity indicate strong coupling superconductivity with the full superconducting gap of $2\Delta(0)/(k_B T_c) = 4.4$ exceeding significantly the weak-coupling BCS limit.^{6,7} Furthermore, muon spin rotation/relaxation (μ SR) experiments show possible multigap or multiband superconductivity⁸ that may originate as a result of the site-selective mechanism involving two Fermi-surface sheets with different band velocities.⁹ In the two independent studies, scanning tunneling spectroscopy was employed to directly probe the multigap behavior of Mo₈Ga₄₁. While measurements on a polycrystalline sample confirmed the two-gap scenario,⁷ study of single crystals revealed the formation of surface domains, where spatially resolved single-gap order parameter was observed.⁹

Besides Mo₈Ga₄₁, there are Mo₆Ga₃₁³ and Mo₄Ga_{21-x-δ}Sn_x⁴ endohedral cluster superconductors, and the latter shows strong coupling superconductivity similar in nature to Mo₈Ga₄₁. Focusing on Mo₆Ga₃₁ with $T_c = 8$ K, its properties are scarcely characterized

in the literature.³ The available information is based on the AC susceptibility and magnetization measurements carried out on a sample with the MoGa₄ nominal composition, which do not correspond to the actual composition of the compound. Moreover, the exact elemental and phase composition of the sample were not reported in Ref.³. The measurements revealed superconductivity of the sample below $T_c = 8$ K in zero magnetic field with the upper critical field of $\mu_0 H_{c2}(0) = 7.4$ T extrapolated to zero temperature.³

Crystal structure of Mo₆Ga₃₁ was probed in two independent studies. In the original investigation, monoclinic crystal structure, the $P2_1/c$ space group, was reported.¹⁰ However, single crystals, which adopt triclinic crystal structure, the $P-1$ space group, were also obtained under different synthetic conditions.¹¹ Both structures of Mo₆Ga₃₁, monoclinic and triclinic, are based on the same building unit, which is shown in Figure 1(a). The main building unit consists of Mo-embedded Mo@Ga₁₀ clusters and Ga-centered Ga@Ga₁₂ cuboctahedra. Twelve Mo@Ga₁₀ clusters form a distorted rectangular superprism, {Mo₁₂Ga₆₂}, where each Mo@Ga₁₀ cluster shares its triangular faces with the Ga@Ga₁₂ cuboctahedron, and two adjacent Ga@Ga₁₂ cuboctahedra have a common rectangular face. In the monoclinic and triclinic structures, these building units connected by corners are perpendicular or codirectional to each other, respectively (Fig. 1(b,c)).

Here, we report on the synthesis, physical properties, and electronic structure of the Mo₆Ga₃₁ endohedral cluster superconductor, a compound, which is closely related to the Mo₈Ga₄₁ and Mo₄Ga_{21-x-δ}Sn_x superconductors in the strong coupling regime. Mo₈Ga₄₁, Mo₆Ga₃₁, and Mo₄Ga_{21-x-δ}Sn_x build up structural series with the general formula of Mo_nGa_{5n+1}, where n corresponds to the

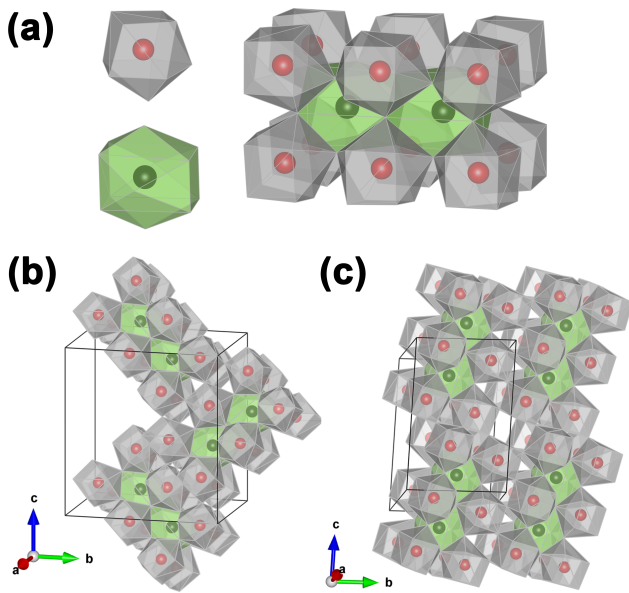


FIG. 1. (a) Main building unit of the $\text{Mo}_6\text{Ga}_{31}$ crystal structure composed of $\text{Mo}@\text{Ga}_{10}$ polyhedra (gray) and $\text{Ga}@\text{Ga}_{12}$ cuboctahedra (green). The arrangement of building units in the monoclinic (b) and triclinic (c) structures is shown in the bottom part of figure.

number of $\text{Mo}@\text{Ga}_{10}$ polyhedra ($\text{Mo}@\text{Ga}_9\text{Sn}$ in the case of $\text{Mo}_4\text{Ga}_{21-x-\delta}\text{Sn}_x$) condensed on one $\text{Ga}@\text{Ga}_{12}$ cuboctahedron in the main building unit. In this study, we investigate the superconducting state of $\text{Mo}_6\text{Ga}_{31}$ in order to measure the electron-phonon coupling and analyze how it correlates with the critical temperature, density of states at the Fermi level, valence electron count and other crucial parameters in the $\text{Mo}_n\text{Ga}_{5n+1}$ series of superconductors.

II. EXPERIMENTAL DETAILS

$\text{Mo}_6\text{Ga}_{31}$ was synthesized using the standard ampule technique. The stoichiometric mixture of Mo (4N, powder) and Ga (5N, pieces) was placed inside a quartz ampule, which was evacuated to the residual pressure of 5×10^{-3} mbar and flame-sealed. To obtain a polycrystalline specimen of $\text{Mo}_6\text{Ga}_{31}$, the ampule was annealed in a programmable furnace at 700°C for 14 days with one intermediate grinding. The resulting black powder, which contains $\text{Mo}_6\text{Ga}_{31}$ with no admixture of other compounds, was used for thermodynamic and electrical transport measurements. Single crystals of $\text{Mo}_6\text{Ga}_{31}$ suitable for structural studies were selected from the specimens prepared under different synthetic conditions employing crystal growth from the high-temperature melt (see Section III.A for details).

High-resolution powder X-ray diffraction (HRPXRD) measurements were performed at the ID22 beam line ($\lambda = 0.35451(1) \text{ \AA}$, $2\theta_{max} = 28^\circ$) of the European Syn-

chrotron Radiation Facility (ESRF, Grenoble, France). Measurements were conducted at room temperature and at elevated temperatures using a hot-air blower on a sample enclosed in a fused silica capillary with a diameter of 0.3 mm. Le Bail fittings of the HRPXRD data were performed using the Jana2006 program.¹² HRPXRD patterns collected at elevated temperatures are presented in the Supporting Information. Polycrystalline specimen of $\text{Mo}_6\text{Ga}_{31}$ was studied by differential scanning calorimetry (DSC) using a STA 409 PC Luxx thermal analyzer (Netzsch). Measurements were performed in high-purity Ar atmosphere at temperatures between 30°C and 600°C with the heating/cooling rate of $10^\circ\text{C}/\text{min}$, and the results are presented in the Supporting Information.

Three-dimensional electron diffraction (3D ED) patterns were collected on a Themis Z transmission electron microscope operated at 300 kV employing the InsteaD-Matic script¹³ for data acquisition. In a typical experiment, a crystal is continuously rotated while ED frames are collected over the tilt range of $\pm 50^\circ$ with the rotation speed of $0.43^\circ/\text{s}$. The exposure time of 0.3 s was used in the experiments. 3D ED patterns were visualized by the REDp program.¹⁴ The collected 3D ED patterns and the corresponding energy-dispersive X-ray (EDX) spectra are presented in the Supporting Information.

Single-crystal X-ray diffraction experiments were performed on a Bruker D8 Venture diffractometer (Mo X-ray source, graphite monochromator, $\lambda = 0.71073 \text{ \AA}$, $T = 100 \text{ K}$) equipped with a Photon 100 CMOS detector. For the absorption correction, the multi-scan routine was employed. The crystal structures were determined by the charge-flipping algorithm using the Superflip program,¹⁵ and refined against $|F^2|$ using the SHELXL-2018¹⁶ and Jana2006 programs.¹² The atomic coordinates were standardized using the STRUCTURE TIDY program¹⁷ as implemented in the VESTA software,¹⁸ which was also used for visualization of crystal structures.

Electronic structure calculations were performed within the framework of density functional theory using the full-potential local-orbital minimum-basis band-structure code FPLO (version 14.00-47).¹⁹ The experimental structural data based on single-crystal XRD measurements were used in calculations. In the scalar relativistic regime, local density approximation was used to treat the exchange and correlation energy.²⁰ Integrations were performed by the improved tetrahedron method²¹ on a grid of $12 \times 12 \times 12$ k -points in the first Brillouin zone.

Electrical resistivity was measured by the standard four-probe technique using the AC transport option of a Physical Property Measurement System (PPMS, Quantum Design) at temperatures between 2 K and 300 K in magnetic fields from 0 T to 10 T. For measurements, a rectangular-shaped pellet with typical dimensions of $8 \times 3 \times 1 \text{ mm}^3$ was prepared by pressing the polycrystalline specimen at the external pressure of 4 kbar at room temperature. Cu wires with the diameter of $100 \mu\text{m}$ were attached to the pellet using silver-containing epoxy resin.

Magnetization measurements were conducted on a Magnetic Properties Measurement System (MPMS 3 SQUID, Quantum Design) in the zero-field-cooling (zfc) and field-cooling (fc) conditions in the temperature range of 1.8–15 K in the magnetic field of 5 Oe. Also, magnetization was measured in the zfc conditions at various fixed temperatures between 2 K and 8 K by sweeping magnetic field from 0 T to 14 T using the VSM option of PPMS. Heat capacity was measured using a relaxation-type calorimeter (HC option of PPMS, Quantum Design) at temperatures between 1.8 K and 20 K in magnetic fields from 0 T to 10 T.

III. RESULTS AND DISCUSSION

A. Synthesis and crystal structure

Although two crystallographic modifications of $\text{Mo}_6\text{Ga}_{31}$ were reported, it is unclear, at which experimental conditions they can be obtained separately. Information on synthesis of the monoclinic $\text{Mo}_6\text{Ga}_{31}$ is missing in the original study,¹⁰ while single crystals of the triclinic $\text{Mo}_6\text{Ga}_{31}$ were obtained from the MoGa_9Si sample, where the $\text{Mo}_6\text{Ga}_{31}$ phase was a side product.¹¹ We systematically studied synthetic conditions, at which single crystals of $\text{Mo}_6\text{Ga}_{31}$ can be obtained. The use of excess of Ga metal leads to crystallization of the $\text{Mo}_8\text{Ga}_{41}$ phase as the main product. Therefore, we performed syntheses of samples with the stoichiometric composition, while controlling the annealing temperature and the cooling rate. The annealing at 700 °C yields polycrystalline $\text{Mo}_6\text{Ga}_{31}$, whereas single crystals can be obtained by increasing the annealing temperature up to 1000 °C. Single crystals of the monoclinic $\text{Mo}_6\text{Ga}_{31}$ were selected from the sample, which was allowed to cool down to room temperature in the shut-off furnace (fast cooling). Single crystals adopting the triclinic structure were found in the sample, which was cooled at the rate of 4 °C/h (slow cooling). In both cases, tiny submillimeter-size single crystals were isolated. The bulk specimen synthesized at 700 °C contains solely polycrystalline $\text{Mo}_6\text{Ga}_{31}$.

Single crystals selected from the specimens were studied by single-crystal X-ray diffraction. Tables S1-S3 of the Supporting Information summarize the results, which are in good agreement with the previous reports,^{10,11} confirming the formation of two crystallographic modifications of $\text{Mo}_6\text{Ga}_{31}$. Here, we comment on the outstanding complexity of the crystal structures: the monoclinic structure contains 38 crystallographic sites [$V = 2566.78(3) \text{ \AA}^3$, $Z = 4$, 148 atoms in the primitive cell], while there are 39 sites in the triclinic structure [$V = 1282.75(2) \text{ \AA}^3$, $Z = 2$, 74 atoms in the primitive cell]. Given this complexity, it is natural to assume the formation of various types of defects in a polycrystalline specimen.

Room-temperature HRPXRD pattern of polycrys-

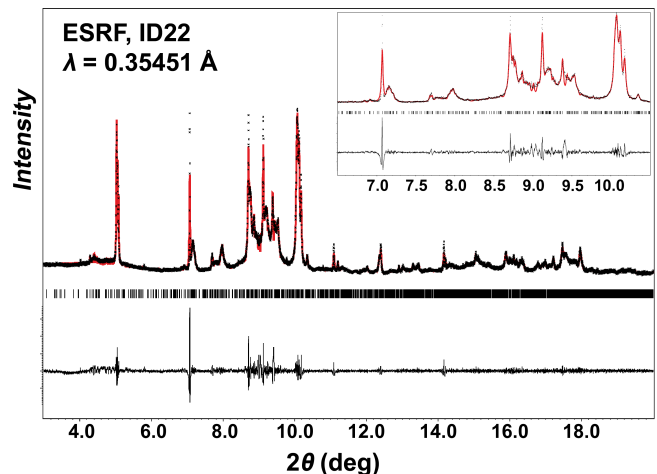


FIG. 2. Experimental (black points) and calculated (red line) HRPXRD patterns of $\text{Mo}_6\text{Ga}_{31}$ at room temperature. Positions of peaks are given by black ticks, and the difference plot is shown by the black line in the bottom part of figure.

talline $\text{Mo}_6\text{Ga}_{31}$ is presented in Figure 2. The pattern shows no secondary compounds, such as $\text{Mo}_8\text{Ga}_{41}$, Mo_3Ga , elemental Mo or Ga. However, all peaks show significant broadening that could be ascribed to defects within the monoclinic phase or to symmetry lowering toward the triclinic structure. Indeed, Le Bail decomposition returned similar profile R factors of $R_p = 6.3$, $R_{wp} = 9.2$, and $GOF = 2.1$ for the monoclinic unit cell, and $R_p = 6.4$, $R_{wp} = 9.3$, and $GOF = 2.2$ for the triclinic unit cell. Under heating up to 700 °C, the HRPXRD pattern remains qualitatively the same, while reflections shift due to the monotonous increase of the lattice parameters. Both temperature-dependent HRPXRD and complementary DSC experiments show no hints for a transformation between the triclinic and monoclinic polymorphs of $\text{Mo}_6\text{Ga}_{31}$ (see Supporting Information).

To gain insight into the local structure of polycrystalline $\text{Mo}_6\text{Ga}_{31}$, three-dimensional electron diffraction was employed providing 3D structural information from nm-size crystals. 3D ED data were collected on crystallites with the lateral size of $< 500 \times 500 \text{ nm}^2$ in order to minimize the contribution of intergrowth and twinning. While testing the lattice type, two types of diffraction patterns with different unit cells were revealed corresponding to the monoclinic and triclinic modifications of $\text{Mo}_6\text{Ga}_{31}$. Unit cell determination by the REDp program^{14,22} yields $a = 9.37(4) \text{ \AA}$, $b = 16.18(6) \text{ \AA}$, $c = 16.48(1) \text{ \AA}$, and $\beta = 94.7(1)^\circ$ for the monoclinic $\text{Mo}_6\text{Ga}_{31}$, and $a = 9.37(5) \text{ \AA}$, $b = 9.47(3) \text{ \AA}$, $c = 14.25(2) \text{ \AA}$, $\alpha = 85.6(2)^\circ$, $\beta = 81.1(1)^\circ$, and $\gamma = 85.7(1)^\circ$ for the triclinic $\text{Mo}_6\text{Ga}_{31}$. Typical 3D ED patterns of the triclinic structure are shown in Figure 3. The unit cell parameters are in good agreement with the single-crystal XRD results within the accuracy of the 3D ED method. EDX spectroscopy does not reveal any difference in the chemical composition of the studied

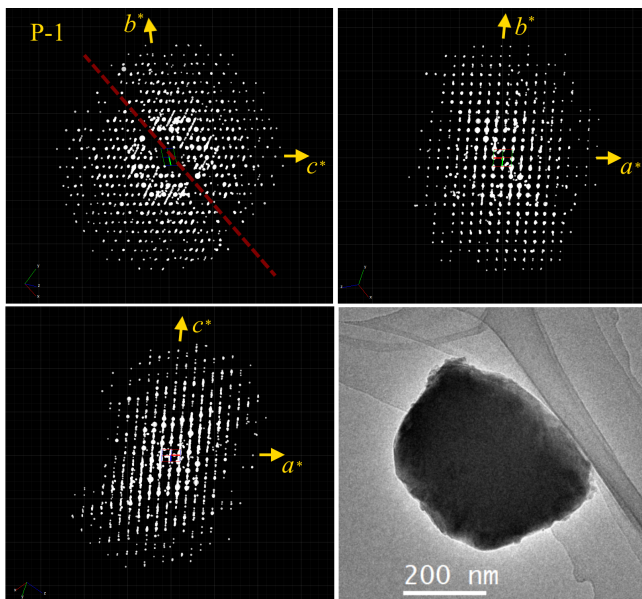


FIG. 3. Experimental 3D ED patterns of the triclinic $\text{Mo}_6\text{Ga}_{31}$, and the corresponding image of crystallite. Red dashed line shows the position of rotation axis towards the reciprocal space of the sample.

crystallites (see Supporting Information). Based on the HRPXRD, DSC, and 3D ED studies, we conclude that both modifications of $\text{Mo}_6\text{Ga}_{31}$ are inherently present in the bulk sample.

B. Electronic structure

Using the structural parameters obtained from the single-crystal XRD data, we calculated electronic structure of $\text{Mo}_6\text{Ga}_{31}$. The triclinic and monoclinic modifications possess qualitatively the same density of states (DOS), which is shown in Figure 4. At low energies between -12 eV and -4 eV , mixing of the Ga $4s$ and $4p$ states is observed with a small contribution of the Mo $4d$ states. At higher energies between -4 eV and 4 eV , the Ga $4p$ and Mo $4d$ states contribute to the total DOS forming the peak substructure. The Fermi level is located at the peak yielding a high value of DOS at $E = E_F$. The calculated electronic structure of $\text{Mo}_6\text{Ga}_{31}$ is similar to that of the $\text{Mo}_8\text{Ga}_{41}$,^{6,9} $\text{Mo}_4\text{Ga}_{21-x-\delta}\text{Sn}_x$,⁴ and $\text{Mo}_7\text{Ga}_{52-x}\text{Zn}_x$ ²³ endohedral cluster compounds, which also possess high DOS at E_F . For $\text{Mo}_6\text{Ga}_{31}$, we find $N(E_F) = 13\text{ st. eV}^{-1}\text{ f.u.}^{-1}$ for the triclinic structure and $17\text{ st. eV}^{-1}\text{ f.u.}^{-1}$ for the monoclinic one. These values yield the bare Sommerfeld coefficient of $31\text{ mJ mol}^{-1}\text{ K}^{-2}$ and $39\text{ mJ mol}^{-1}\text{ K}^{-2}$, respectively. For the reported endohedral cluster superconductors, the value of the density of states at the Fermi level correlates with the observed critical temperature.^{1,4} Given the high DOS at $E = E_F$ calculated for $\text{Mo}_6\text{Ga}_{31}$, which is comparable with those of the $\text{Mo}_8\text{Ga}_{41}$ and $\text{Mo}_4\text{Ga}_{21-x-\delta}\text{Sn}_x$ su-

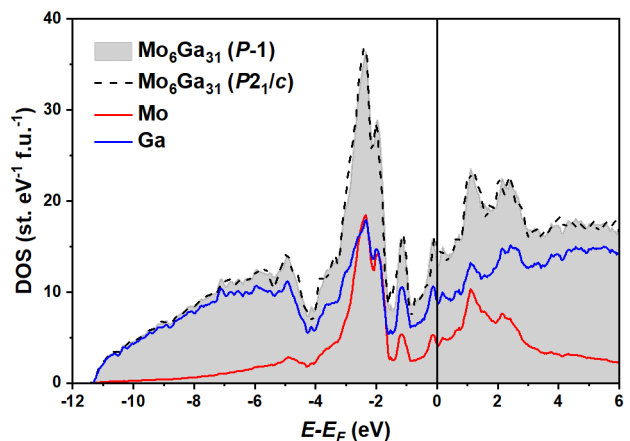


FIG. 4. Electronic structure of the triclinic $\text{Mo}_6\text{Ga}_{31}$. Total density of states is shown by the shaded area, the Mo and Ga contributions – by the solid red and blue lines, respectively. The density of states of the monoclinic structure is shown by the dashed line. The position of the Fermi level is indicated by the solid black line.

perconductors, we expect superconducting behavior for both crystallographic modifications of $\text{Mo}_6\text{Ga}_{31}$. However, triclinic and monoclinic $\text{Mo}_6\text{Ga}_{31}$ should possess slightly different superconducting-state parameters, including the critical temperature, T_c , and full superconducting gap, $2\Delta(0)/(k_B T_c)$. Our HRPXRD and 3D ED studies show that the triclinic and monoclinic structures are in strong contact with each other in the bulk specimen. Due to the proximity effect,²⁴ the superconducting carriers travel coherently between two superconducting phases, and thus, intermediate superconducting parameters should be observed, corresponding effectively to one superconducting phase.

C. Physical properties

Electrical resistivity of $\text{Mo}_6\text{Ga}_{31}$ follows metallic behavior at elevated temperatures. However, the $\rho(T)$ dependence is extremely flat between 10 K and 300 K , and shows the saturation behavior with increasing temperature. The small residual-resistance-ratio of 1.2 can be paralleled to the peak broadening observed in HRPXRD and caused by the coexisting domains of the monoclinic and triclinic phases. At low temperatures, superconducting transition is observed with the low-temperature drop of resistivity occurring between the onset temperature of 8.2 K and the final temperature of 7.8 K in zero magnetic field. The increase of magnetic field shifts the transition to lower temperatures, and finally, no indications of superconductivity are observed at temperatures above 1.8 K in the magnetic field of $\mu_0 H = 10\text{ T}$.

The bulk nature of superconductivity is confirmed by thermodynamic measurements (Fig. 6). Dimensionless volume magnetic susceptibility shows diamagnetic shift

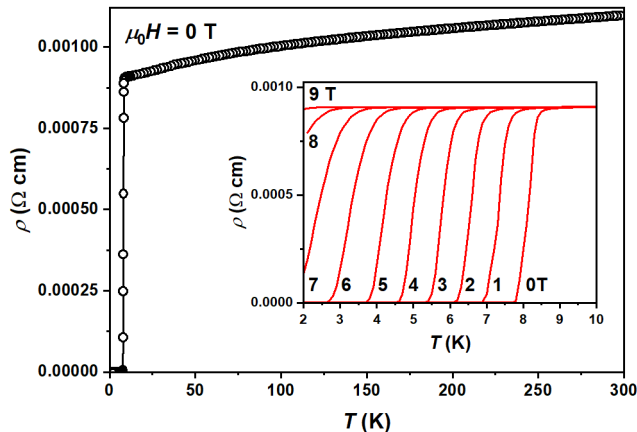


FIG. 5. Electrical resistivity of $\text{Mo}_6\text{Ga}_{31}$ in zero magnetic field. The inset shows the data at low temperatures in magnetic fields between 0 T and 9 T.

due to the Meissner effect below the critical temperature of $T_c = 8.2$ K in 5 Oe magnetic field. The zfc signal of -0.94 at the lowest measured temperature indicates large volume fraction of the superconducting phase. The transition is broad with temperature and shows a pronounced shoulder, which is presumably caused by the inhomogeneities of the specimen. Volume magnetization, which is shown in the inset of Figure 6, is characteristic of type-II superconductors. Note that the logarithmic scale is used in figure to represent the magnetic fields. In low magnetic fields, $4\pi M_V$ follows the linear behavior versus $\mu_0 H$ below the lower critical field of $\mu_0 H_{c1} = 70$ Oe at $T = 2$ K. With the increase of magnetic field, the normal state is achieved above the upper critical field of $\mu_0 H_{c2} = 6.5$ T at $T = 2$ K. Between $\mu_0 H_{c1}$ and $\mu_0 H_{c2}$, the volume magnetization exhibits intricate nonmonotonic behavior, which also evidences the presence of inhomogeneities in the specimen.

The specific heat of $\text{Mo}_6\text{Ga}_{31}$ exhibits the superconducting anomaly located at $T_c = 8.2$ K in zero magnetic field in good agreement with the resistivity and magnetization measurements. The increase of the magnetic field shifts the transition to lower temperatures, which simultaneously becomes smoothed (Fig. 7). The temperature sweeps of resistivity and heat capacity measured in various magnetic fields, as well as the field sweeps of magnetization at constant temperatures were used to extract the upper critical field of $\text{Mo}_6\text{Ga}_{31}$ as a function of temperature (Fig. 8). The $\mu_0 H_{c2}(T)$ values, which correspond to the onset temperature of the resistivity drop, are larger than those from the magnetization and heat capacity measurements indicating the so-called $\mu_0 H_{c3}(T)$ upper critical field of the surface superconductivity, which was also observed in the case of $\text{Mo}_8\text{Ga}_{41}$.⁶ From the other hand, the temperatures, at which zero resistance is achieved, yields $\mu_0 H_{c2}(T)$, which are closer to the thermodynamic measurements. The magnetization and heat-capacity derived $\mu_0 H_{c2}(T)$ values are in good

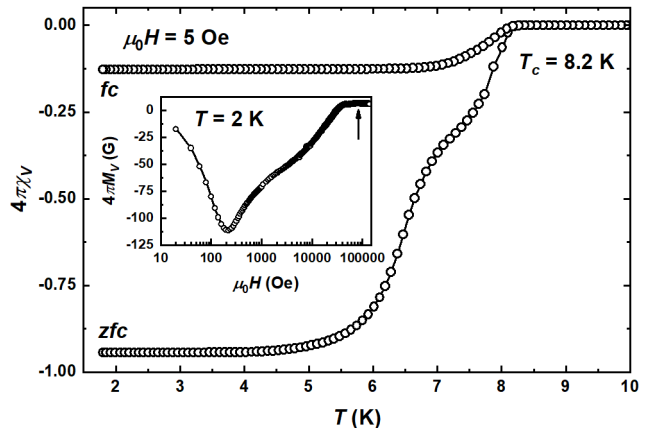


FIG. 6. Dimensionless volume magnetic susceptibility of $\text{Mo}_6\text{Ga}_{31}$ measured in 5 Oe magnetic field in the zfc and fc conditions. The inset shows volume magnetization measured at $T = 2$ K. The arrow indicates the transition to the normal state.

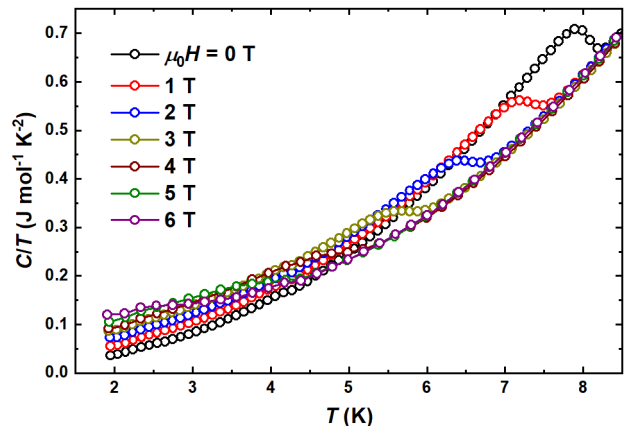


FIG. 7. Specific heat of $\text{Mo}_6\text{Ga}_{31}$ in various magnetic fields.

agreement with each other. Above these values, the bulk of the sample is in the normal state. Interpolation of the $\mu_0 H_{c2}(T)$ values by the second-order polynomial yields $\mu_0 H_{c2}(0) = 7.8$ T at zero temperature, which is in good agreement with the previous report.³ The $\mu_0 H_{c2}(0)$ value corresponds to the Ginzburg-Landau coherence length of $\xi = 153$ Å as calculated from the equation $\mu_0 H_{c2}(0) = \frac{\Phi_0}{2\pi\xi_{GL}^2}$, where $\Phi_0 = h/2e$ is the flux quantum. At temperatures above 6 K, $\mu_0 H_{c2}(T)$ is linear with the slope of $\omega = -1.2$ T K⁻¹. According to the Werthamer-Helfand-Honenberg (WHH) model, the upper critical field can be calculated as $\mu_0 H_{c2}(0) = -0.693\omega T_c = 6.8$ T, which is smaller than the extrapolated value of $\mu_0 H_{c2}(0) = 7.8$ T. This enhancement of the upper critical field may be due to strong electron-phonon coupling.

To gain insight into the electron-phonon coupling in the superconducting state of $\text{Mo}_6\text{Ga}_{31}$, the specific heat data were analyzed. Figure 9 shows the spe-

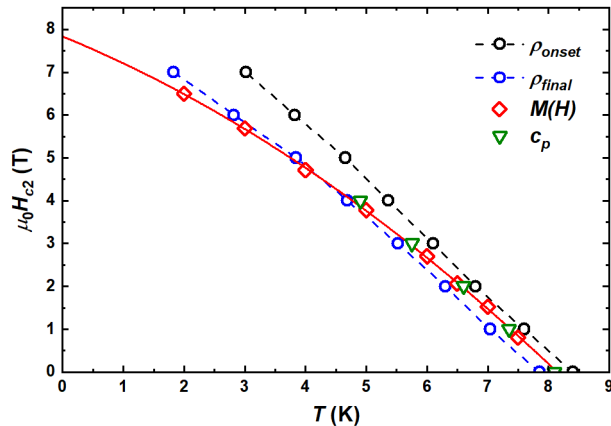


FIG. 8. Upper critical field of $\text{Mo}_6\text{Ga}_{31}$.

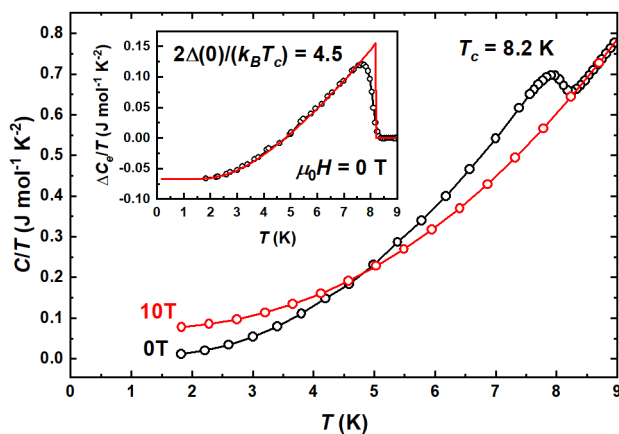


FIG. 9. Specific heat of $\text{Mo}_6\text{Ga}_{31}$ measured in 0 T and 10 T magnetic fields. The inset shows the electronic contribution to the total heat capacity in zero magnetic field. The red line is a fit according to the α -model.

cific heat in superconducting ($\mu_0 H = 0$ T) and normal states ($\mu_0 H = 10$ T). The electronic specific heat, which is shown in the inset of Figure 9, was calculated as $\Delta C_e/T = \Delta C/T(0\text{ T}) - \Delta C/T(10\text{ T})$ and analyzed within the BCS-derived α -model.^{25,26} The fitting yields the full superconducting gap of $2\Delta(0)/(k_B T_c) = 4.5$, the normalized specific heat jump of $\Delta C_e/(\gamma_N T_c) = 2.3$ at $T = T_c$, and the normal-state Sommerfeld coefficient of $\gamma_N = 67\text{ mJ mol}^{-1}\text{ K}^{-2}$. Remarkably, the transition is smoothed with temperature, which is seen as the difference between the experimental data (black open circles in the inset of Fig. 9) and the calculated specific heat (solid red line) in the vicinity of the critical temperature, which may be caused by the coexisting domains of the monoclinic and triclinic phases. Both the enhanced value of $\Delta C_e/(\gamma_N T_c) = 2.3$, which is larger than the weak-coupling BCS limit of $\Delta C_e/(\gamma_N T_c) = 1.43$, and the large value of $\alpha = 2.25$ point to the strong electron-phonon coupling in the superconducting state. Using the

TABLE I. Normal- and superconducting-state parameters of the $\text{Mo}_8\text{Ga}_{41}$,^{6,7} $\text{Mo}_6\text{Ga}_{31}$, and $\text{Mo}_4\text{Ga}_{21-x-\delta}\text{Sn}_x$ ⁴ endohedral cluster superconductors. m refers to the monoclinic polymorph of $\text{Mo}_6\text{Ga}_{31}$, and t to triclinic.

Parameter	$\text{Mo}_8\text{Ga}_{41}$	$\text{Mo}_6\text{Ga}_{31}$	$\text{Mo}_4\text{Ga}_{21-x-\delta}\text{Sn}_x$
T_c (K)	9.8	8.2	5.85
VEC (e per Mo)	21.375	21.5	21.85
$\mu_0 H_{c2}$ (T) at $T = 2$ K	7.45	6.5	1.9
$2\Delta(0)/(k_B T_c)$	4.4	4.5	4.1
γ_N ($\text{mJ mol}^{-1}\text{ K}^{-2}$)	99	67	39
γ_{bare} ($\text{mJ mol}^{-1}\text{ K}^{-2}$)	52.7	$31.1^t/39.1^m$	20.0
λ_{ep}	0.9	$1.15^t/0.7^m$	0.95

bare Sommerfeld coefficient of $\gamma_{bare} = 31.1\text{ mJ mol}^{-1}\text{ K}^{-2}$ (triclinic structure) and $39.1\text{ mJ mol}^{-1}\text{ K}^{-2}$ (monoclinic structure), the electron-phonon coupling constant can be calculated as $\lambda_{ep} = \frac{\gamma_N}{\gamma_{bare}} - 1$, which yields $\lambda_{ep} = 1.15$ and 0.7 for the triclinic and monoclinic modifications, respectively. Both values suggest strong or moderate electron-phonon coupling. Thus, $\text{Mo}_6\text{Ga}_{31}$ is a strongly-coupled superconductor similar to the $\text{Mo}_8\text{Ga}_{41}$ and $\text{Mo}_4\text{Ga}_{21-x-\delta}\text{Sn}_x$ related compounds.^{4,6,7}

In Table I, we compare normal- and superconducting-state properties of $\text{Mo}_8\text{Ga}_{41}$, $\text{Mo}_6\text{Ga}_{31}$, and $\text{Mo}_4\text{Ga}_{21-x-\delta}\text{Sn}_x$. The observed T_c values follow the trend of decreasing the critical temperature with increasing the valence electron count (VEC), which was proposed for endohedral cluster superconductors.¹ Moreover, it is obvious that the critical temperature correlates with the value of DOS at $E = E_F$: both γ_N and γ_{bare} decrease with decreasing T_c . At the same time, the values of full superconducting gap, $2\Delta(0)/(k_B T_c)$, and electron-phonon coupling constant, λ_{ep} , almost do not vary in the series indicating that the strength of the electron-phonon coupling in the superconducting state has no significant impact on the critical temperature.

IV. CONCLUSIONS

In the paper, synthesis, structural characteristics, computational electronic structure, and physical properties of the $\text{Mo}_6\text{Ga}_{31}$ superconductor are reported. The bulk type-II superconductivity is observed below the critical temperature of 8.2 K in zero magnetic field, and below the upper critical field of 7.8 T extrapolated to zero temperature. Remarkably, the superconducting state is in the strong-coupling regime with the large ratio of $2\Delta/(k_B T_c) = 4.5$. This places $\text{Mo}_6\text{Ga}_{31}$ in line with the $\text{Mo}_8\text{Ga}_{41}$ and $\text{Mo}_4\text{Ga}_{21-x-\delta}\text{Sn}_x$ superconductors, for which the strong electron-phonon coupling was also reported. Interestingly, the critical temperature correlates with the composition in the $\text{Mo}_8\text{Ga}_{41}$ ($T_c = 9.8\text{ K}$), $\text{Mo}_6\text{Ga}_{31}$ (8.2 K), and $\text{Mo}_4\text{Ga}_{21-x-\delta}\text{Sn}_x$ (5.85 K) series, namely, with the number of Mo atoms per formula unit, and with the density of states at the Fermi level. In the

listed superconductors, Mo is placed inside the Mo@Ga₁₀ endohedral clusters, where strong mixing of the Mo *4d* states and Ga *4p* states yields peculiar electronic structure in the vicinity of the Fermi energy. The high density of states is observed at $E = E_F$, which may be favorable for superconductivity. Moreover, the framework composed of Mo@Ga₁₀ clusters exhibits specific phonon properties that give rise to the strong electron-phonon coupling. Thus, Mo₆Ga₃₁ expands the family of Mo-based strongly-coupled superconductors.

ACKNOWLEDGMENTS

The authors acknowledge the European Synchrotron Radiation Facility for granting the beam time and thank Dr. Wilson Mogodi for his help during the high-resolution PXR experiments. The work was supported by the Russian Science Foundation, grant no. 17-13-01033. V.Yu.V. acknowledges the financial support from the Mobilitas program of the European Science Foundation, grant no. MOBJD449. A.A.T. appreciates financial support by the Federal Ministry for Education and Research under the Sofja Kovalevskaya Award of the Alexander von Humboldt Foundation. Z.W. and E.V.D. thank the National Science Foundation for supporting structural studies under grant no. CHE-1152441.

-
- * valeriy.verchenko@gmail.com
- ¹ W. Xie, H. Luo, B. F. Phelan, T. Klimczuk, F. A. Cevallos, and R. J. Cava, *Proc. Natl. Acad. Sci. USA* **112**, E7048 (2015).
 - ² A. Bezinge, K. Yvon, M. Decroux, and J. Muller, *J. Less-Common Met.* **99**, L27 (1984).
 - ³ O. Fischer, *Helvetica Physica Acta* **45**, 331 (1972).
 - ⁴ V. Y. Verchenko, A. O. Zhubtsovskii, Z. Wei, A. A. Tsirlin, M. Marcin, A. V. Sobolev, I. A. Presniakov, E. V. Dikarev, and A. V. Shevelkov, *Inorg. Chem.* **58**, 15552 (2019).
 - ⁵ T. Shibayama, M. Nohara, H. A. Katori, Y. Okamoto, Z. Hiroi, and H. Takagi, *J. Phys. Soc. Jpn.* **76**, 073708 (2007).
 - ⁶ V. Y. Verchenko, A. A. Tsirlin, A. O. Zhubtsovskiy, and A. V. Shevelkov, *Phys. Rev. B* **93**, 064501 (2016).
 - ⁷ M. Marcin, J. Kačmarčík, Z. Pribulová, M. Kopčík, P. Szabó, O. Šofranko, T. Samuely, V. Vaňo, C. Marcecat, V. Y. Verchenko, A. V. Shevelkov, and P. Samuely, *Sci. Rep.* **9**, 13552 (2019).
 - ⁸ V. Y. Verchenko, R. Khasanov, Z. Guguchia, A. A. Tsirlin, and A. V. Shevelkov, *Phys. Rev. B* **96**, 134504 (2017).
 - ⁹ A. Sirohi, S. Saha, P. Neha, S. Das, S. Patnaik, T. Das, and G. Sheet, *Phys. Rev. B* **99**, 054503 (2019).
 - ¹⁰ K. Yvon, *Acta Cryst. B* **30**, 853 (1974).
 - ¹¹ R. Lux, *Dissertation: Intermetallische Verbindungen mit hochschmelzenden Übergangsmetallen und niedrigschmelzenden Metallen* (University of Freiburg, Freiburg, Germany, 2004).
 - ¹² V. Petříček, M. Dušek, and L. Palatinus, *Z. Kristallogr.* **229**, 345 (2014).
 - ¹³ M. Roslova, S. Smeets, B. Wang, T. Thersleff, H. Xu, and X. Zou, “Towards cross-platform automated rotation electron diffraction,” (2019), arXiv:1911.09393.
 - ¹⁴ W. Wan, J. Sun, J. Su, S. Hovmöller, and X. Zou, *J. Appl. Cryst.* **46**, 1863 (2013).
 - ¹⁵ L. Palatinus and G. Chapius, *J. Appl. Cryst.* **40**, 786 (2007).
 - ¹⁶ G. M. Sheldrick, *Acta Crystallogr., Sect. C: Struct. Chem.* **C71**, 3 (2015).
 - ¹⁷ L. M. Gelato and E. Parthé, *J. Appl. Cryst.* **20**, 139 (1987).
 - ¹⁸ K. Momma and F. Izumi, *J. Appl. Cryst.* **44**, 1272 (2011).
 - ¹⁹ K. Koepf and H. Eschrig, *Phys. Rev. B* **59**, 1743 (1999).
 - ²⁰ J. P. Perdew and Y. Wang, *Phys. Rev. B* **45**, 13244 (1992).
 - ²¹ P. E. Blöchl, O. Jepsen, and O. K. Andersen, *Phys. Rev. B* **49**, 16223 (1994).
 - ²² W. Kabsch, *Acta Cryst. D* **66**, 125 (2010).
 - ²³ V. Y. Verchenko, A. O. Zhubtsovskii, Z. Wei, A. A. Tsirlin, E. V. Dikarev, and A. V. Shevelkov, *Dalton Trans.* **48**, 7853 (2019).
 - ²⁴ C. P. Poole, *Handbook of Superconductivity* (Academic Press, 525 B Street, Suite 1900, San Diego, CA 92101-4495, USA, 2000).
 - ²⁵ H. Padamsee, J. E. Neighbor, and C. A. Shiffman, *J. Low Temp. Phys.* **12**, 387 (1973).
 - ²⁶ D. C. Johnston, *Supercond. Sci. Technol.* **26**, 115011 (2013).